LIVER CANCER

Macrophage inflammatory protein-2 contributes to liver resection-induced acceleration of hepatic metastatic tumor growth

Otto Kollmar, Michael D Menger, Martin K Schilling

Otto Kollmar, Martin K Schilling, Department of General, Visceral, Vascular and Pediatric Surgery, University of the Saarland, D-66421 Homburg/Saar, Germany
Michael D Menger, Institute for Clinical and Experimental Surgery, University of the Saarland, D-66421 Homburg/Saar, Germany
Supported by the grants of the Research Committee and the Medical Faculty of the University of Saarland, No. HOMFOR-A/2003/1
Correspondence to: Otto Kollmar, MD, Department of General, Visceral, Vascular and Pediatric Surgery, University of the Saarland, D-66421 Homburg/Saar, Germany. chokol@uniklinik-saarland.de
Telephone: +49-6841-1622611 Fax: +49-6841-1622697
Received: 2005-07-22 Accepted: 2005-08-26

Abstract

AIM: To study the role of macrophage inflammatory protein (MIP)-2 in liver resection-induced acceleration of tumor growth in a mouse model of hepatic metastasis.

METHODS: After a 50% hepatectomy, 1×10^5 CT26.WT cells were implanted into the left liver lobe of syngeneic balb/c mice (PHx). Additional animals were treated with a monoclonal antibody (MAB452) neutralizing MIP-2 (PHx+mAB). Non-resected and non-mAB-treated mice (Con) served as controls. After 7 d, tumor angiogenesis and microcirculation as well as cell proliferation, tumor growth, and CXCR-2 expression were analyzed using intravital fluorescence microscopy, histology, immunohistochemistry, and flow cytometry.

RESULTS: Partial hepatectomy increased ($P < 0.05$) the expression of the MIP-2 receptor CXCR-2 on tumor cells when compared with non-resected controls, and markedly accelerated ($P < 0.05$) angiogenesis and metastatic tumor growth. Neutralization of MIP-2 by MAB452 treatment significantly ($P < 0.05$) depressed CXCR-2 expression. Further, the blockade of MIP-2 reduced the angiogenic response ($P < 0.05$) and inhibited tumor growth ($P < 0.05$). Of interest, liver resection-induced hepatocyte proliferation was not effected by anti-MIP-2 treatment.

CONCLUSION: MIP-2 significantly contributes to liver resection-induced acceleration of colorectal CT26.WT hepatic metastasis growth.

INTRODUCTION

Major liver resection initiates rapid regeneration and growth of the remaining liver to restore the functional hepatic capacity[1]. The cellular changes which provoke liver regeneration are orchestrated by a complex network of different growth factors, cytokines[1-3] and chemokines[4-6]. The latter include macrophage inflammatory protein (MIP)-2, ENA-78, and IL-8, which all may act through the CXCR-2 receptor. The role of this receptor has been shown in that blockade with antibodies or deletion in gene-targeted animals significantly reduced the regeneration after hepatectomy[4,6]. The role of the individual chemokines in regeneration after hepatectomy, however, may be redundant. The murine CXC chemokine MIP-2 is a functional analog of human IL-8[7]. Similar to IL-8, it acts as a potent neutrophil chemoattractant, contributing to wound healing[8] and inflammation[9]. While blockade of the chemokine receptor CXCR-2 decreases regeneration of the residual liver, neutralization of MIP-2 through the use of anti-MIP-2 antibodies did not affect the process of regeneration as indicated by the unchanged liver weight to body weight (BW) ratios[4]. These findings indicate that other chemokines may replace or act via the CXCR-2 receptor in case of MIP-2 deletion for liver regeneration[4,6].

Besides parenchymal regeneration, hepatectomy also accelerates tumor growth in the remaining liver[10-14] as well as in remote organ sites[15]. Slooter and co-workers showed that a 70% liver resection provokes excessive growth of liver metastases when compared to non-resected controls. Of interest, the intravenous application of TNF-α was effective to significantly reduce these outgrowths of tumor masses[11]. In fact, the acceleration of tumor growth seems to be proportional to the volume of the resected

liver tissue[10,11,13]. The cause of enhanced tumor growth in the liver after hepatectomy is likely to be multifactorial. It has been suggested that, besides mechanisms of liver regeneration, residual "dormant" micrometastases or tumor cells in the remnant liver are stimulated through distinct pro-tumorigenic factors[13,14]. In addition, a depression of local defense mechanisms due to a decrease of Kupffer cell tumoricidal activity and systemic immune paralysis may also contribute to the enhancement of tumor growth[16]. The role of chemokines, such as MIP-2, in the hepatectomy-induced acceleration of tumor growth, however, has not been elucidated yet.

By use of a murine colorectal hepatic metastasis model, we studied whether the accelerated metastatic growth after hepatectomy is mediated by the CXC chemokine MIP-2, and whether the inhibition of tumor growth by blockade of MIP-2 is associated with a downregulation of angiogenesis and tumor blood vessel formation.

MATERIALS AND METHODS

Experiments were performed after approval by the local governmental ethic committee, and were in accordance with the UKCCCR Guidelines for the Welfare of Animals in Experimental Neoplasia (*Br J Cancer* 1998; 77: 1-10) and the Interdisciplinary Principles and Guidelines for the Use of Animals in Research (New York Academy of Sciences Ad Hoc Committee on Animal Research, NY, USA).

Tumor cell line and culture conditions

The CT26 cell line is an *N*-nitroso-*N*-methylurethane-induced undifferentiated adenocarcinoma of the colon, syngeneic with the BALB/c mouse. For our studies, the CT26.WT cell line (ATCC CRL-2638®, LGC Promochem GmbH, Wesel, Germany) was grown in cell culture as monolayers in RPMI-1640 medium with 2 mmol/L L-glutamine (Sigma Aldrich Chemie GmbH, Taufkirchen, Germany) supplemented with 10% fetal calf serum (FCS Gold, PAA Laboratories GmbH, Cölbe, Germany), 100 U/mL penicillin and 100 μg/mL streptomycin (PAA Laboratories GmbH). The cells were incubated at 37°C in a humidified atmosphere containing 50 mL/L CO_2 in air. Only cells of the first two serial passages after cryo-storage were used. At the day of implantation, CT26.WT cells were harvested from sub-confluent cultures (70%-85%) by trypsinization (0.5 g/L trypsin and 0.2 g/L EDTA, PAA Laboratories GmbH), and washed twice in phosphate-buffered saline solution (PBS, PAA Laboratories GmbH) before being resuspended in PBS at 1×10^7 cells/L.

Flow cytometric analysis of CT26.WT cells

FACScan (Becton Dickinson, Mountain View, CA, USA) analysis was performed to assess the expression of the chemokine receptor CXCR-2 of the CT26.WT cells. After trypsinization, the cells were fixed in 1 mL Cytofix/Cytoperm (BD Biosciences, Heidelberg, Germany) for 20 min at 4°C, washed twice with Perm Wash (BD Biosciences) and incubated at room temperature for 40 min with a polyclonal rabbit anti-mouse CXCR-2 antibody (Santa Cruz, Heidelberg, Germany) or an isotype-matched control antibody (Dianova, Hamburg, Germany). A goat anti-rabbit Cy3-conjugated antibody (1:25; Dianova) was used for fluorescence labeling. To remove excess of antibody, cells were washed again and were then maintained in 10 g/L paraformaldehyde in PBS. Flow cytometry was performed within the next 3 h. The FACScan flow cytometer was calibrated with fluorescent standard microbeads (CaliBRITE Beads, BD Biosciences) for accurate instrument setting. Tumor cells were selectively analyzed for their fluorescence properties using the CellQuest data handling program (BD Biosciences) with the assessment of 5 000 events per sample.

Hepatectomy and tumor cell implantation

Eight to twelve weeks old female BALB/c mice with a BW of 18-20 g, kept in a temperature and humidity controlled 12-h light/dark cycle environment, were used. The animals were anesthetized by intraperitoneal injection of 25 mg/kg BW xylazin hydrochloride (Rompun®, Bayer, Leverkusen, Germany) and 125 mg/kg BW ketamine hydrochloride (Ketavet®, Pharmacia GmbH, Erlangen, Germany). The anesthetized animals were placed in supine position. After laparotomy through a midline incision, a 50% hepatectomy was performed. After ligature of the supplying and draining blood vessels with PDS 5-0 (Ethicon, Johnson & Johnson Company, Norderstedt, Germany), the right lateral lobes (ventral and dorsal), the right medial lobe and a part of the left medial lobe were resected. The weight of the resected tissue was 0.35 ± 0.01 g. The procedure of intrahepatic implantation of CT26.WT tumor cells was performed as described previously[17]. The left liver lobe was gently mobilized and 1×10^5 tumor cells in 10 μL PBS were implanted under the capsule of the lower surface using a 25-μL syringe with a 32-G needle (Gastight® #1702, Hamilton Bonaduz AG, Bonaduz, Switzerland). The puncture site was sealed with acrylic glue (Histoacryl®, B. Braun, Aesculap AG, Tuttlingen, Germany), and the left liver lobe was repositioned anatomically into the peritoneal cavity. The abdominal wall was closed by a one layer technique with a polypropylene suture (Prolene® 5-0).

Intravital fluorescence microscopy

At d 7 after tumor cell implantation, the animals were again anesthetized and laparotomized. The left liver lobe with the tumor was exteriorized and placed on an adjustable stage, so that the lower surface of the lobe was positioned horizontally to the microscope. This guaranteed adequate focus levels for the *in vivo* fluorescence microscopy procedure. The surface of the lobe was covered with a cover slip to avoid drying of the tissue and influences of the ambient oxygen[17]. *In vivo* fluorescence microscopy was performed by epi-illumination technique using a modified Zeiss Axiotech microscope (Zeiss, Oberkochen, Germany)[18]. Microscopic images were monitored by a charge-coupled device video camera (FK 6990, Prospective Measurements Inc., San Diego, CA, USA) and were transferred to a video system (VO-5800 PS, Sony, München, Germany) for subsequent off-line analysis. Angioarchitecture and microvascular perfusion were analyzed after intravenous contrast enhancement with sodium fluorescein (2 μmol/kg; Merck, Darmstadt,

Germany) using blue light epi-illumination (450 to 490 nm > 520nm, excitation and emission wavelengths).

Microcirculation analysis

Assessment of hepatic microcirculatory parameters was performed off-line by frame-to-frame analysis of the videotaped images using a computer-assisted image analysis system (CapImage; Zeintl, Heidelberg, Germany). Sinusoidal, capillary and venular diameters (µm) were measured perpendicularly to the vessel path. Sinusoidal density within the liver and capillary density within the tumors (cm/cm²) were determined by measuring the length of red cell perfused capillary per area of observation. The number of venules draining the blood flow from the tumor was counted and was given per tumor margin. The angiogenic front neighboring the tumor margin, characterized by newly developed, chaotically arranged capillaries, was measured in mm² surface area.

Morphological examinations

At the end of the experiment, the left liver lobe was harvested and cut into slices with a diameter of 1 mm using a Tissue Slicer (McIlwain Tissue Shopper, Saur Laborbedarf, Reutlingen, Germany). Slices were documented with the use of a stereo-microscope (Leica M651, Leica Microsystems AG, Heerbrugg, Switzerland) and a video system, and the size of the tumor was measured with CapImage according to: tumor volume (mm³) $= 4/3\pi \times a/2 \times b/2 \times c/2$ (a, b, and c represent the three perpendicularly orientated diameters of the tumor).

Histochemistry and immunohistochemistry

For light microscopy, formalin-fixed biopsies were embedded in paraffin. Five micrometer thick sections were cut and stained with hematoxylin and eosin for routine histology according to standard procedures.

Proliferating cell nuclear antigen (PCNA) staining was performed using indirect immunoperoxidase techniques. Therefore, deparaffinized sections were incubated with 30 mL/L H_2O_2 to block endogenous peroxidases and with 20 mL/L goat normal serum for blocking unspecific binding sites. A monoclonal mouse anti-pan PCNA antibody (PC10, 1:50; DakoCytomation, Hamburg, Germany) was used as primary antibody. A biotinylated goat anti-mouse rabbit IgG antibody was used as secondary antibody for streptavidin-biotin-complex peroxidase staining (1:200, LSAB 2 System HRP, DakoCytomation). 3,3'-Diaminobenzidine (DakoCytomation) was used as a chromogen. Sections were counterstained with hemalaun according to Mayer and examined by light microscopy.

For CXCR-2 immunohistochemistry tumor slices were embedded in Tissue Freezing Medium (Jung; Leica Microsystems, Nussloch, Germany), snap-frozen in liquid nitrogen and stored at -80 °C. Five micrometer thick cryostat sections were cut, fixed in 4 °C cold acetone for 5 s followed by fixation in 16 g/L formaldehyde for 10 min and blocked with 2% normal donkey serum. Tissue sections were then incubated with the polyclonal rabbit anti-mouse CXCR-2 antibody (1:100; Santa Cruz, CA, USA). A donkey anti-rabbit IgG HRP conjugated antibody (1:500; Amersham, Freiburg, Germany) was used as secondary antibody. 3,3'-Diaminobenzidine was used as chromogen. Sections were counterstained with hemalaun according to Mayer and examined by light microscopy. As a negative control, additional slices from each specimen were exposed to appropriate IgG isotype-matched antibody (Sigma Aldrich Chemie GmbH) in place of primary antibody under the same conditions to determine the specificity of antibody binding. All of the control stainings were found negative.

Experimental protocol

A total of 21 animals received tumor cell implantation and were assigned to three different groups. Animals without liver resection and without further treatment received tumor cell implantation in the left liver lobe and served as controls (Con; $n = 7$). In the additional two groups ($n = 7$ each), a 50% hepatectomy was performed before the tumor cells were implanted into the left liver lobe. One group of animals (PHx+mAB) received 1 mg/kg BW of the monoclonal rat anti-mouse MIP-2 antibody (MAB452, R&D Systems, Wiesbaden, Germany) at the day of operation and every second day thereafter. Untreated animals with 50% liver resection served as hepatectomy controls (PHx). Seven days after tumor cell implantation and treatment, all animals underwent intravital microscopic examination and the liver and tumor tissue were harvested for histology and immunohistochemistry.

Statistical analysis

All values were expressed as mean ± SE. After proving the assumption of normality and homogeneity of variance across groups, differences between groups were calculated by a one-way analysis of variance (ANOVA) followed by a *post hoc* Student-Newman-Keuls test, including correction of the alpha error to compensate for multiple comparisons. Overall statistical significance was set at $P < 0.05$. Statistical analysis was performed with the use of the software package SigmaStat (SPSS Inc., Chicago, IL, USA).

RESULTS

Tumor growth

Tumor cell implantation, hepatectomy and treatment with the anti-mouse MIP-2 antibody did not affect the general conditions of the animals. All animals had an uneventful postoperative recovery, and, regardless of the group, animals did not show significant changes of BW during the 7-d experimental period. Intravital fluorescence microscopy at d 7 after tumor cell implantation showed that hepatectomy (PHx) provoked a significant ($P < 0.05$) acceleration of tumor growth, as indicated by an increased tumor area at the surface of the liver when compared with that of controls (Figure 1). Analysis of the tumor volume confirmed the significantly ($P < 0.05$) increased tumor growth, demonstrating a tumor mass which was 18-fold greater than that of controls (Figure 1). Treatment with the MIP-2 antibody (PHx+mAB) was capable of significantly ($P < 0.05$) reducing the hepatectomy-induced acceleration of tumor growth, resulting in a tumor volume which was only 6-fold of that of non-resected controls (Figure 1).
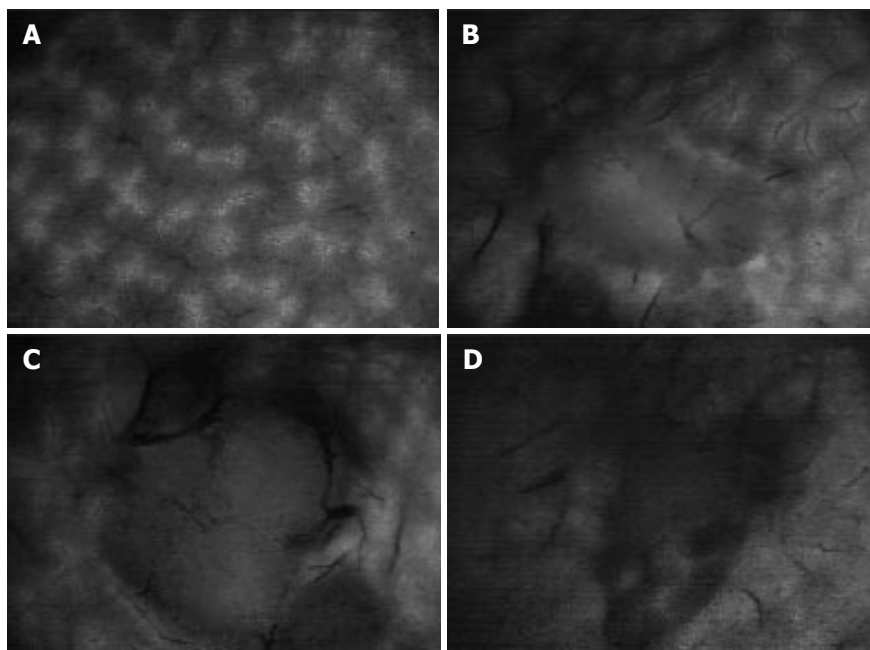
Figure 1 Intravital fluorescence microscopy at d 7 after tumor cell implantation. **A:** Displays the normal liver microvasculature; **B:** shows the microvasculature of the tumor of a non-resected control animal (Con); **C:** displays a 7-day tumor and its microvasculature of an animal which underwent hepatectomy (PHx); **D:** shows the tumor microvasculature after additional anti-MIP-2 treatment (PHx+mAB). Quantitative analysis of tumor area (**E**) and tumor volume (**F**) showed that hepatectomy (PHx) markedly accelerated tumor growth when compared with controls (Con), and that additional anti-MIP-2 treatment (PHx+mAB) was capable of significantly reducing this liver resection-induced tumor growth. Mean ± SE; [a]$P < 0.05$ *vs* Con; [c]$P < 0.05$ *vs* PHx. Magnifications (**A-D**) ×16.
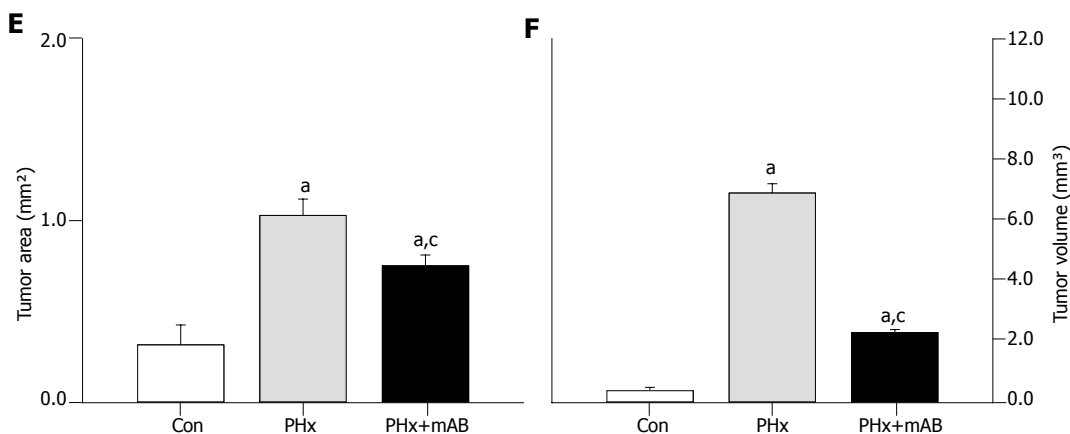
Angiogenesis and microangioarchitecture

Intravital fluorescence microscopy revealed that normal liver presents with a regularly arranged architecture of sinusoids and homogeneous staining of parenchymal cell nuclei (Figure 1A). In contrast, the center of the tumor showed a density of capillaries which was markedly lower than that of the sinusoids in the normal liver (Figure 1 and 2). The margin of the tumor showed an angiogenic front with newly developed, chaotically arranged capillaries (Figure 2) and large draining venules (Figure 3). In control animals, the implantation of CT26.WT cells induced an area of the tumor surrounding angiogenic front of 0.33 mm² at day 7 (Figure 2). Hepatectomy (PHx) significantly increased the area of the angiogenic front by 3-fold ($P < 0.05$) when compared with that of controls. Blockade of MIP-2 (PHx+mAB) was capable of inhibiting angiogenesis, as indicated by a significantly ($P < 0.05$) reduced area at the tumor margin which showed new blood vessel development (Figure 2D).

Because angiogenesis is regularly associated with vasodilation, we analyzed the capillary diameters within the angiogenic front. Within the tumor margin, hepatectomy (PHx) induced a significant dilation of the newly formed capillaries ($P < 0.05$) when compared with that of controls.

Additional anti-MIP-2 treatment (PHx+mAB) further pronounced ($P < 0.05$) this dilatory effect (Figure 2E). Of interest, the enlargement of the newly formed capillaries within the angiogenic front after hepatectomy and MIP-2 treatment was a homogeneous response, as indicated by the fact that the coefficient of variance of capillary diameters did not differ when compared with untreated controls (Figure 2F). Further, hepatectomy (PHx) also significantly ($P < 0.05$) increased the density of venules draining the tumor, as indicated by a 6.5-fold increase of the number of venules within the tumor margin when compared to controls (Figure 3). These venules were also found enlarged in diameter (Figure 3E), however, without increased heterogeneity when compared with controls (Figure 3F). Interestingly, blockade of MIP-2 significantly ($P < 0.05$) reduced the number of draining tumor venules when compared with animals undergoing only hepatectomy (Figure 3D).

Tumor morphology

Hematoxylin-eosin-stained sections revealed solid growth of the colorectal CT26.WT hepatic metastasis in all the animals (Figure 4). Satellite metastases were not observed in the left liver lobe. In the control group, tumors were
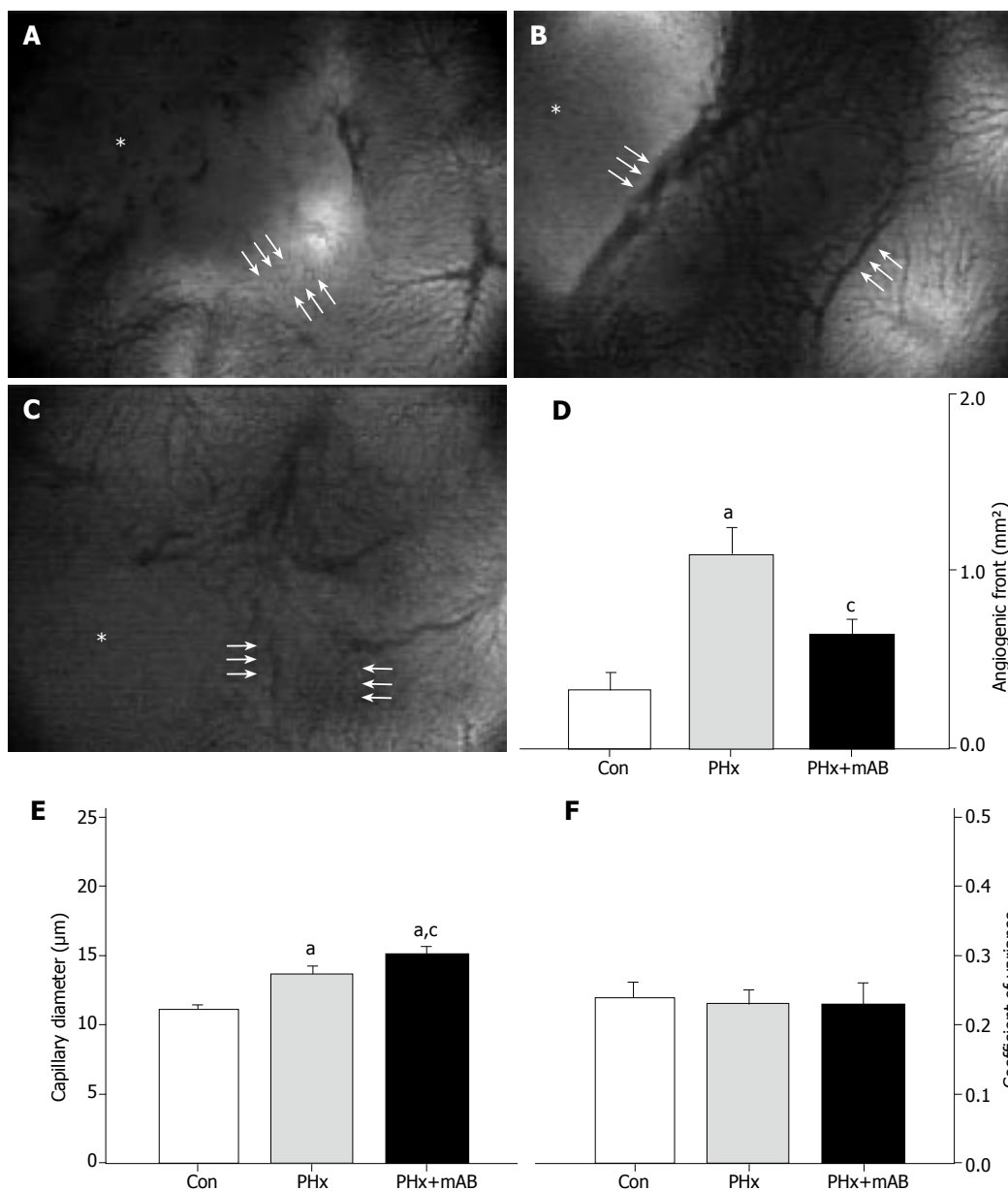
Figure 2 Analysis of the size of the angiogenic front (area between the triple arrows) at the margin of tumors (asterisks) in control mice (**A**, Con), after hepatectomy (**B**, PHx) and after hepatectomy and additional anti-MIP-2 treatment (**C**, PHx+mAB). Quantitative analysis of the area of the angiogenic front (**D**) indicated a significant increase after hepatectomy (PHx) when compared with that of controls (Con). Additional anti-MIP-2 treatment (PHx+mAB) was capable of reducing the angiogenic process. Further, hepatectomy (PHx) significantly increased capillary dilation within the angiogenic front (**E**) compared to controls (Con), which was even more pronounced after additional anti-MIP-2 treatment (PHx+mAB). The heterogeneity of capillary diameters, as given by the coefficient of variance, was not affected in either of the treatment groups (**F**). Mean ± SE; [a]$P < 0.05$ *vs* Con; [c]$P < 0.05$ *vs* PHx. Magnifications (**A-C**) ×40.

round in nature with a homogeneous appearance, however, with aggressive growth characteristics (Figures 4A and B). Hepatectomy (PHx) accelerated tumor growth, resulting in enlarged tumors with a dense arrangement of tumor cells in the center (Figures 4C and D). In two of the seven animals, lung metastases could be detected macroscopically, although no additional metastases could be found in the abdominal cavity. In contrast, tumors of animals, which additionally were treated with anti-MIP-2 showed central cell death via either necrotic or apoptotic pathways (Figures 4E and F). In this group tumor growth at distant sites was not observed.

In vitro FACScan analysis and CXCR-2 expression *in vivo*

FACScan analysis showed that 98.8% of the CT26.WT cells were CXCR-2 receptor positive *in vitro* (Figure 5). *In vivo*, CXCR-2 immunohistochemistry revealed that - 40% of the tumor cells were receptor-positive. The majority of these CXCR-2 expressing cells were located within the tumor margin (Figure 6). Quantitative analysis of CXCR-2 expression indicated that hepatectomy (PHx)

significantly increased ($P < 0.05$) CXCR-2 expression to -60% of tumor cells (Figure 6). Blockade of MIP-2 (PHx +mAB) not only abolished the hepatectomy-induced increase of CXCR-2 expression, but further reduced ($P < 0.05$) CXCR-2 expression on tumor cells to only -10% (Figure 6).

Proliferation of tumor cells and normal liver

PCNA as an indicator of cell proliferation showed that >90% of tumor cells displayed strong PCNA staining (Figure 7). By this, the tumor sharply demarcated from the surrounding liver tissue. Notably, neutralization of MIP-2 (PHx+mAB) decreased the rate of PCNA-positive cells to -60% (Figures 7C and D), indicating a reduction of proliferation by deletion of MIP-2 function. Normal liver tissue only occasionally showed single PCNA-positive cells (Figure 8). Hepatectomy (PHx) resulted in a significant ($P < 0.05$) increase of the number of PCNA-stained cells when compared with that of non-resected controls (Figure 8). Of interest, additional blockade of MIP-2 induced
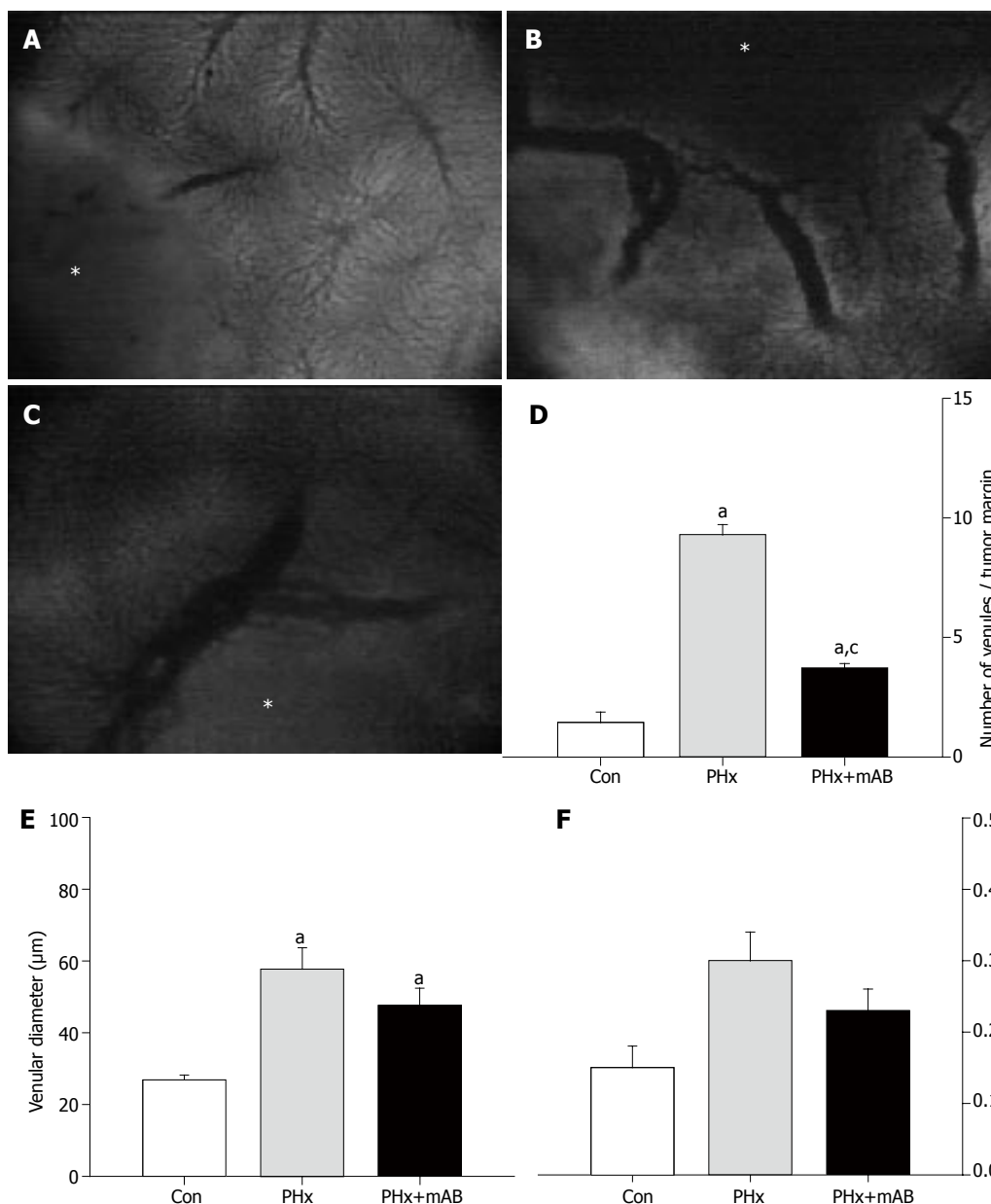
Figure 3 Analysis of the number of venules within the margin of tumors (**A-C**, asterisk) of control mice (A, Con), after hepatectomy (**B**, PHx) and after hepatectomy and additional anti-MIP-2 treatment (**C**, PHx+mAB). Quantitative analysis showed that hepatectomy significantly increases the number of venules (**D**), and causes a marked dilation of the draining venules within the margin of the tumors (**E**). Additional anti-MIP-2 treatment was capable of significantly reducing the liver resection-induced increase of the number of tumor venules (**D**). The heterogeneity of venular diameters, as given by the coefficient of variance, was not affected in either of the treatment groups (**F**). Mean ± SE; [a]$P<0.05$ *vs* Con; [c]$P<0.05$ *vs* PHx. Magnifications (**A-C**) ×40.

a further increase ($P<0.05$) of the fraction of PCNA-positive cells in the normal liver (Figure 8).

DISCUSSION

The major findings of the present study are that (1) MIP-2 significantly promotes liver resection-induced expression of the chemokine receptor CXCR-2, and (2) blockade of MIP-2 blunts the augmentation of angiogenesis and metastatic tumor growth after hepatectomy. This indicates for the first time a significant role of this chemokine in the acceleration of tumor growth after hepatectomy. The rodent liver fully regenerates within 8 d after resection[19,20]. The setpoint for growth regulation is the ratio between liver mass and body mass rather than liver mass *per se*[1]. Using a 70% liver resection model in mice, Drixler *et al.* demonstrated that liver regeneration is accompanied by intrahepatic angiogenesis[20]. Liver resection has also been shown to affect the immune system in the early phase of liver regeneration[3]. The MIP-2-CXCR-2 system is thought

to be involved in the hepatic regenerative processes after extended resection[4,6]. While blockade of the chemokine receptor CXCR-2 decreases regeneration of the residual liver, selective neutralization of MIP-2 through the use of anti-MIP-2 antibodies is not affecting the liver-to-BW ratio[4]. Of interest, CXCR-2 seems to be pivotal, because other chemokines may replace or act via the CXCR-2 receptor in case of MIP-2 deletion for liver regeneration[4,6].

After resection of colorectal liver metastases, diseases recur in over two-thirds of the patients[21]. This observation indicates that undetected residual microscopic tumors remain in the majority of patients undergoing curative hepatectomy[22]. The locally released factors which trigger the process of regeneration after hepatectomy may even augment the outgrowth of these residual microtumors, thus, additionally contributing to the high rate of recurrences. This view is supported by experimental studies, demonstrating that liver resection enhances tumor growth during regeneration[11,13,14,16]. Using different rat hepatectomy models, these authors suggested
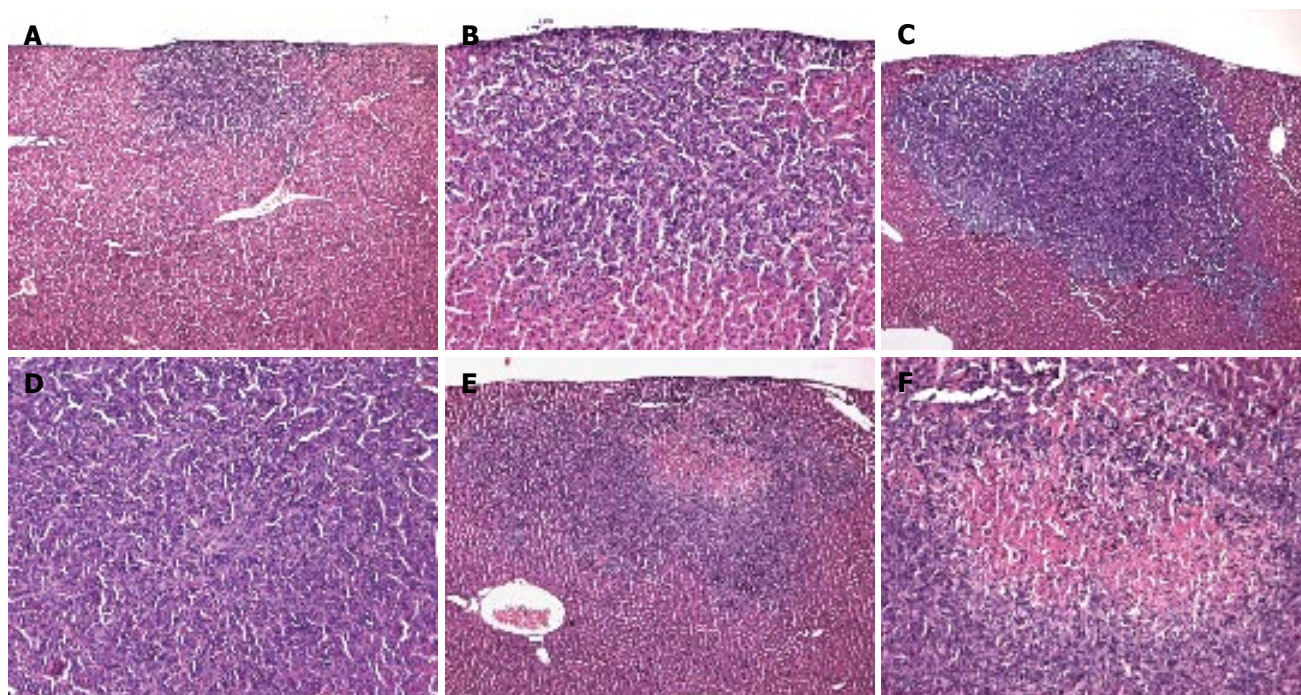
Figure 4 Hematoxylin–eosin-staining of tumors of a control mouse (**A** and **B**), a mouse which underwent hepatectomy (PHx) (**C** and **D**), and a mouse which additionally received anti-MIP-2 treatment (**E** and **F**). Sections revealed solid growth of the colorectal CT26.WT hepatic metastasis in all the animals. Tumors were round in nature, however, showed aggressive growth characteristics. Anti-MIP-2 treatment provoked an area of necrosis within the tumor center (**E** and **F**). Magnifications (**A**, **C** and **E**) ×18, (**B**, **D** and **F**) ×88.
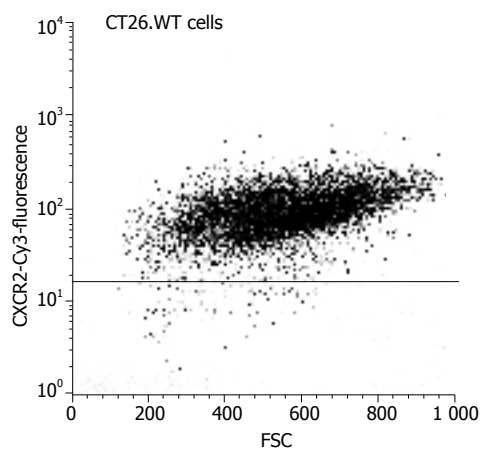
Figure 5 FACScan analysis of CT26.WT cells, demonstrating positive staining and thus expression of the chemokine receptor CXCR-2 by almost all of the tumors cells studied.

that immunoparalysis with lack of Kupffer cell function and TNF-α response as well as overproduction of growth factors, such as TGF-α, TGF-β and bFGF, contribute to the acceleration of tumor growth.

For the first time, we have herein demonstrated that MIP-2 is involved in hepatectomy-induced metastatic tumor growth. So far, little is known about the role of MIP-2 in tumorigenesis. A recent study indicated that the reduction of fibrosarcoma growth by inhibiting lymphotoxin-β receptor can be reconstituted through co-transfection with MIP-2[23]. The mechanism how MIP-2 is involved in the herein observed liver resection-induced acceleration of tumor growth seems to be the pro-proliferative action of this chemokine, because neutralization of MIP-2 significantly reduced PCNA expression on the tumor cells. Of interest, regeneration of the normal liver was not affected by the anti-MIP-2 treatment, inasmuch as hepatocyte PCNA expression after resection was found even increased when compared with that of untreated hepatectomized controls. This is in line with other experimental studies, which demonstrate that blockade of MIP-2 alone did not affect the process of regeneration[4].

In the present study, we have shown that *in vitro* almost all CT26.WT cells expressed the CXC receptor CXCR-2. *In vivo*, approximately 40% of the cells of non-treated CT26 tumors showed positive CXCR-2 staining 7 days after tumor cell implantation. The reduction of the number of CXCR-2 positive cells is probably due to the fact that solid tumors *in vivo* consist besides the CT26.WT clone of a variety of other cells, including endothelia, fibroblasts and stromal cells, which do not necessarily express CXCR-2. Furthermore, we have demonstrated for the first time that over a 7-d period partial hepatectomy increased the expression of CXCR-2 to -60%. Because receptor expression seems to be required for the proliferative action of chemokines on tumors[24], the increased *in vivo* expression of CXCR-2 may represent the mechanism of action of the MIP-2-associated acceleration of tumor growth after hepatectomy. The neutralization of MIP-2 by MAB452 significantly reduced CXCR-2 expression within the tumor. Although we cannot exclude that neutralization of MIP-2 directly alters the CXCR-2 expression of tumor cells, the histological findings may additionally suggest a relative increase of CXCR-2-negative stromal cells.

The progressive growth of a malignant solid tumor depends on the development of new blood vessels. The
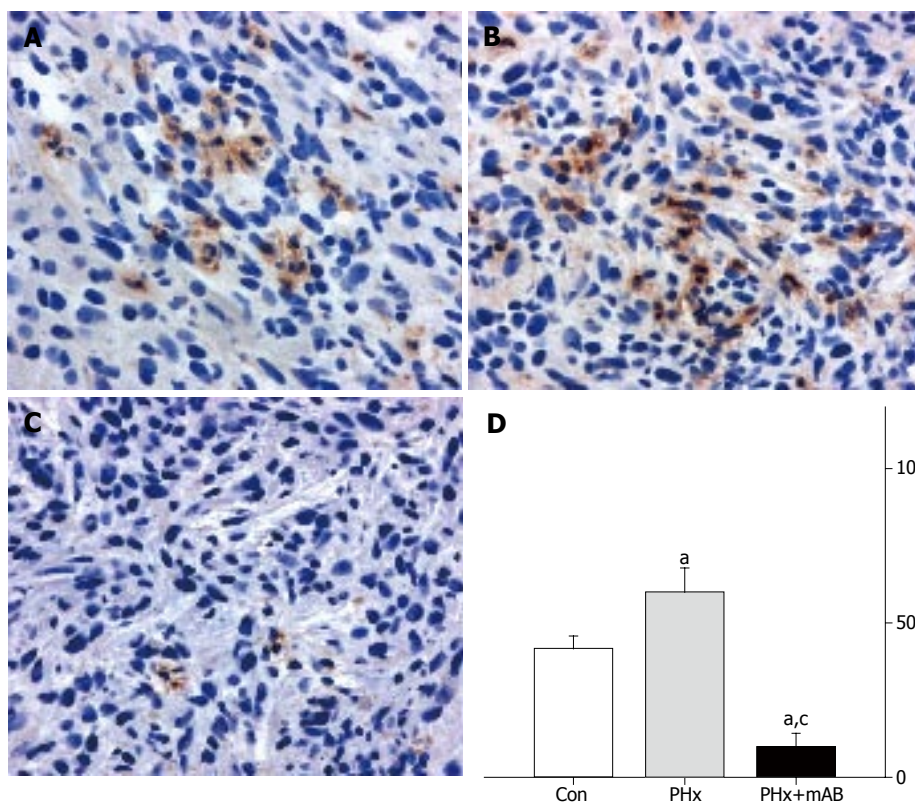
Figure 6 CXCR-2 immunohistochemistry and quantitative analysis of the number of receptor-positive cells (given in percent of all cells) revealed that within tumors of control animals (Con) ~40% of the cells express CXCR-2 (**A** and **D**). Hepatectomy (PHx) significantly increased CXCR-2 expression to ~60% (**B** and **D**). Of interest, additional blockade of MIP-2 (PHx+mAB) significantly reduced tumor cell CXCR-2 expression and inhibits significantly the liver resection-induced increase of CXCR-2 expression (**C** and **D**). Mean±SE; [a]$P < 0.05$ *vs* Con; [c]$P < 0.05$ *vs* PHx. Magnifications (**A-C**) ×175.
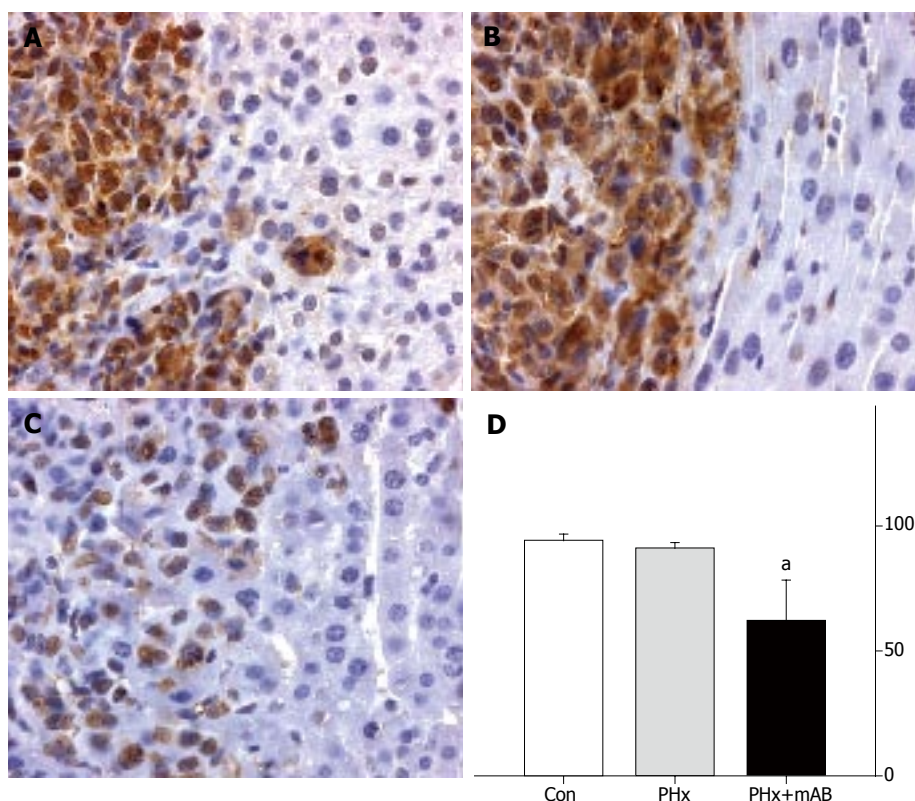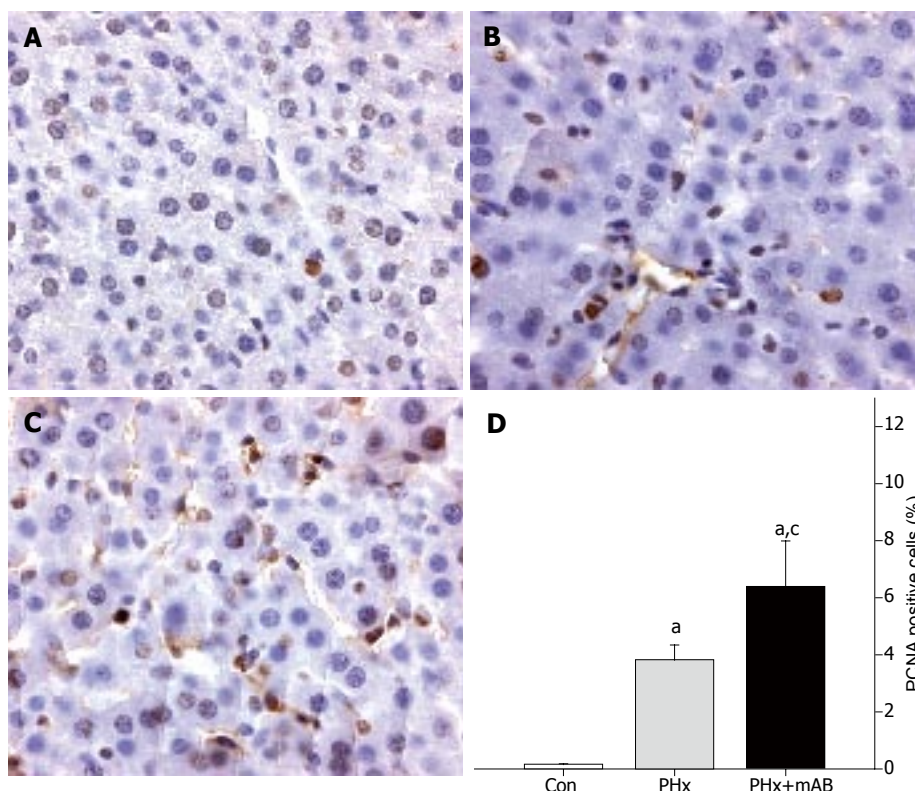

Figure 7 PCNA immunohistochemistry and quantitative analysis of the number of PCNA-positive cells (given in percent of all cells) in liver tumors of control mice (**A**, Con), after hepatectomy (**B**, PHx), and after hepatectomy and additional anti-MIP-2 treatment (**C**, PHx+mAB). Tumor cells display massive PCNA staining, in particular to those located within the tumor margin. By this, these positive cells sharply demarcate the tumor from the surrounding liver tissue (**A**, **B**, and **C**). Quantitative analysis revealed that neutralization of MIP-2 significantly reduces the number of PCNA-positive tumor cells (**D**). Mean±SE; [a]$P < 0.05$ *vs* Con. Magnifications (**A-C**) ×175.

tumor vasculature is chaotically organized and does not follow a hierarchical branching pattern of normal vascular networks[25]. As a result of this abnormal organization, the diameters of those tumor vessels are irregular, the blood flow is heterogeneous, and the endothelial lining is leaky[25]. In the present study, the tumor microvasculature presented with a marked heterogeneity, as indicated by a relatively high coefficient of variance of capillary and venular diameter within the angiogenic front. This is in line with the results of previous reports, which also demonstrated markedly irregular vessel diameters of tumors grown from other colon cancer cell lines at ectopic sites different from that of the liver[26].

CXC chemokines with the three amino acids Glu-

Figure 8 PCNA immunohistochemistry of normal liver tissue of control mice (**A**, Con), after hepatectomy (**B**, PHx), and after hepatectomy and additional anti-MIP-2 treatment (**C**, PHx+mAB). Quantitative analysis revealed that hepatectomy increases the number of PCNA-positive stained cells when compared to controls (**D**). Additional neutralization of MIP-2 further enhanced the number of PCNA-positive cells (**D**). Mean ± SE; $^aP < 0.05$ vs Con; $^cP < 0.05$ vs PHx. Magnifications (**A-C**) ×175.

Leu-Arg immediately amino-terminal to the CXC motif (ELR+) are thought to be angiogenic, while CXC (ELR –) chemokines are angiostatic[27]. There is no information, however, on whether the CXC (ELR+) chemokine MIP-2 is involved in angiogenesis of tumors. In inflammation, Scapini et al[28] demonstrated that MIP-2 induces angiogenesis in vivo and that this is mediated by the neutrophil-derived vascular endothelial growth factor-A. In addition, Keane et al[29] showed that neutralization of MIP-2 by monoclonal antibodies inhibits the bleomycin-induced angiogenic activity in lung specimens. The present study provides evidence that MIP-2 is also involved in tumor angiogenesis, because the inhibition of the chemokine blunted the liver resection-induced acceleration of new blood vessel formation.

The mechanisms of inhibition of angiogenesis by blockade of MIP-2 are not clarified yet. Our intravital microscopic studies demonstrate that the hepatectomy-mediated increase in angiogenesis is associated with pronounced dilation of the newly formed microvessels. Although we have not studied the mechanism of this dilatory response, it may be speculated that it is caused by the action of VEGF, which is capable of inducing distinct vasodilation, in particular in ischemic tissue[30]. VEGF is known as the predominant inductor of tumor angiogenesis and its promoter is preferentially activated within the angiogenic front of the tumor margin[31]. This effect, however, cannot be attributed to the action of MIP-2, because anti-MIP-2 treatment could not abolish the liver-resection-induced dilation of the newly formed microvessels.

In the present study we found that inhibition of MIP-2 induced central cell death within the tumors. Previous studies on inflammation have demonstrated that apoptotic cells are capable of enhancing secretion of MIP-2 by macrophages, triggering an inflammatory response to remove cell debris[32,33]. Accordingly, the functional inhibition of MIP-2 in our experiments may have prevented the recruitment of inflammatory cells, and, thus avoided the removal of the cell debris from the center of the tumors.

In conclusion, we have demonstrated that MIP-2 significantly promotes liver resection-induced acceleration of angiogenesis and metastatic tumor growth. Our results therefore indicate that the neutralization of MIP-2 may be a potential strategy for additional anti-tumor therapy in patients undergoing liver resection.

ACKNOWLEDGMENTS

REFERENCES

1   **Fausto N.** Liver regeneration. *J Hepatol* 2000; **32:** 19-31
2   **Kren BT,** Trembley JH, Fan G, Steer CJ. Molecular regulation of liver regeneration. *Ann N Y Acad Sci* 1997; **831:** 361-381
3   **Sato Y,** Farges O, Buffello D, Bismuth H. Intra- and extrahepatic leukocytes and cytokine mRNA expression during liver regeneration after partial hepatectomy in rats. *Dig Dis Sci* 1999; **44:** 806-816
4   **Ren X,** Carpenter A, Hogaboam C, Colletti L. Mitogenic properties of endogenous and pharmacological doses of macrophage inflammatory protein-2 after 70% hepatectomy in the mouse. *Am J Pathol* 2003; **163:** 563-570
5   **Hogaboam CM,** Bone-Larson CL, Steinhauser ML, Lukacs NW, Colletti LM, Simpson KJ, Strieter RM, Kunkel SL. Novel CXCR2-dependent liver regenerative qualities of ELR-containing CXC chemokines. *FASEB J* 1999; **13:** 1565-1574
6   **Colletti LM,** Green M, Burdick MD, Kunkel SL, Strieter RM.

Proliferative effects of CXC chemokines in rat hepatocytes in vitro and in vivo. *Shock* 1998; **10**: 248-257

7   **Oppenheim JJ,** Zachariae CO, Mukaida N, Matsushima K. Properties of the novel proinflammatory supergene "intercrine" cytokine family. *Annu Rev Immunol* 1991; **9**: 617-648

8   **Fahey TJ 3rd,** Sherry B, Tracey KJ, van Deventer S, Jones WG 2nd, Minei JP, Morgello S, Shires GT, Cerami A. Cytokine production in a model of wound healing: the appearance of MIP-1, MIP-2, cachectin/TNF and IL-1. *Cytokine* 1990; **2**: 92-99

9   **Schramm R,** Thorlacius H. Neutrophil recruitment in mast cell-dependent inflammation: inhibitory mechanisms of glucocorticoids. *Inflamm Res* 2004; **53**: 644-652

10   **Mizutani J,** Hiraoka T, Yamashita R, Miyauchi Y. Promotion of hepatic metastases by liver resection in the rat. *Br J Cancer* 1992; **65**: 794-797

11   **Slooter GD,** Marquet RL, Jeekel J, Ijzermans JN. Tumour growth stimulation after partial hepatectomy can be reduced by treatment with tumour necrosis factor alpha. *Br J Surg* 1995; **82**: 129-132

12   **Drixler TA,** Borel Rinkes IH, Ritchie ED, van Vroonhoven TJ, Gebbink MF, Voest EE. Continuous administration of angiostatin inhibits accelerated growth of colorectal liver metastases after partial hepatectomy. *Cancer Res* 2000; **60**: 1761-1765

13   **Picardo A,** Karpoff HM, Ng B, Lee J, Brennan MF, Fong Y. Partial hepatectomy accelerates local tumor growth: potential roles of local cytokine activation. *Surgery* 1998; **124**: 57-64

14   **Panis Y,** Ribeiro J, Chretien Y, Nordlinger B. Dormant liver metastases: an experimental study. *Br J Surg* 1992; **79**: 221-223

15   **Schindel DT,** Grosfeld JL. Hepatic resection enhances growth of residual intrahepatic and subcutaneous hepatoma, which is inhibited by octreotide. *J Pediatr Surg* 1997; **32**: 995-997; discussion 997-998

16   **Karpoff HM,** Jarnagin W, Delman K, Fong Y. Regional muramyl tripeptide phosphatidylethanolamine administration enhances hepatic immune function and tumor surveillance. *Surgery* 2000; **128**: 213-218

17   **Kollmar O,** Schilling MK, Menger MD. Experimental liver metastasis: standards for local cell implantation to study isolated tumor growth in mice. *Clin Exp Metastasis* 2004; **21**: 453-460

18   **Menger MD,** Marzi I, Messmer K. In vivo fluorescence microscopy for quantitative analysis of the hepatic microcirculation in hamsters and rats. *Eur Surg Res* 1991; **23**: 158-169

19   **Michalopoulos GK,** DeFrances MC. Liver regeneration. *Science* 1997; **276**: 60-66

20   **Drixler TA,** Vogten MJ, Ritchie ED, van Vroonhoven TJ, Gebbink MF, Voest EE, Borel Rinkes IH. Liver regeneration is an angiogenesis- associated phenomenon. *Ann Surg* 2002; **236**: 703-711; discussion 711-712

21   **Fong Y,** Fortner J, Sun RL, Brennan MF, Blumgart LH. Clinical score for predicting recurrence after hepatic resection for metastatic colorectal cancer: analysis of 1001 consecutive cases. *Ann Surg* 1999; **230**: 309-318; discussion 318-321

22   **Delman KA,** Zager JS, Bennett JJ, Malhotra S, Ebright MI, McAuliffe PF, Halterman MW, Federoff HJ, Fong Y. Efficacy of multiagent herpes simplex virus amplicon-mediated immunotherapy as adjuvant treatment for experimental hepatic cancer. *Ann Surg* 2002; **236**: 337-342; discussion 342-343

23   **Hehlgans T,** Stoelcker B, Stopfer P, Muller P, Cernaianu G, Guba M, Steinbauer M, Nedospasov SA, Pfeffer K, Mannel DN. Lymphotoxin-beta receptor immune interaction promotes tumor growth by inducing angiogenesis. *Cancer Res* 2002; **62**: 4034-4040

24   **Zeelenberg IS,** Ruuls-Van Stalle L, Roos E. The chemokine receptor CXCR4 is required for outgrowth of colon carcinoma micrometastases. *Cancer Res* 2003; **63**: 3833-3839

25   **Jain RK.** Molecular regulation of vessel maturation. *Nat Med* 2003; **9**: 685-693

26   **Leunig M,** Yuan F, Menger MD, Boucher Y, Goetz AE, Messmer K, Jain RK. Angiogenesis, microvascular architecture, microhemodynamics, and interstitial fluid pressure during early growth of human adenocarcinoma LS174T in SCID mice. *Cancer Res* 1992; **52**: 6553-6560

27   **Homey B,** Muller A, Zlotnik A. Chemokines: agents for the immunotherapy of cancer? *Nat Rev Immunol* 2002; **2**: 175-184

28   **Scapini P,** Morini M, Tecchio C, Minghelli S, Di Carlo E, Tanghetti E, Albini A, Lowell C, Berton G, Noonan DM, Cassatella MA. CXCL1/macrophage inflammatory protein-2-induced angiogenesis in vivo is mediated by neutrophil-derived vascular endothelial growth factor-A. *J Immunol* 2004; **172**: 5034-5040

29   **Keane MP,** Belperio JA, Moore TA, Moore BB, Arenberg DA, Smith RE, Burdick MD, Kunkel SL, Strieter RM. Neutralization of the CXC chemokine, macrophage inflammatory protein-2, attenuates bleomycin-induced pulmonary fibrosis. *J Immunol* 1999; **162**: 5511-5518

30   **Takeshita S,** Isshiki T, Ochiai M, Eto K, Mori H, Tanaka E, Umetani K, Sato T. Endothelium-dependent relaxation of collateral microvessels after intramuscular gene transfer of vascular endothelial growth factor in a rat model of hindlimb ischemia. *Circulation* 1998; **98**: 1261-1263

31   **Fukumura D,** Xavier R, Sugiura T, Chen Y, Park EC, Lu N, Selig M, Nielsen G, Taksir T, Jain RK, Seed B. Tumor induction of VEGF promoter activity in stromal cells. *Cell* 1998; **94**: 715-725

32   **Lucas M,** Stuart LM, Savill J, Lacy-Hulbert A. Apoptotic cells and innate immune stimuli combine to regulate macrophage cytokine secretion. *J Immunol* 2003; **171**: 2610-2615

33   **Hohlbaum AM,** Gregory MS, Ju ST, Marshak-Rothstein A. Fas ligand engagement of resident peritoneal macrophages in vivo induces apoptosis and the production of neutrophil chemotactic factors. *J Immunol* 2001; **167**: 6217-6224